The X-ray Photoelectron Spectra of Ir, IrO_2 and $IrCl_3$ Revisited

S. J. Freakley, J. Ruiz-Esquius and D. J. Morgan*

Cardiff Catalysis Institute, School of Chemistry, Park Place, Cardiff. CF10 3AT. UK

Email: MorganDJ3@cardiff.ac.uk

*Corresponding Author

Keywords: XPS, Iridium, IrO_2, fitting, oxide, CasaXPS

Abstract

The X-ray photoelectron spectra of metallic iridium and the technologically important iridium compounds, IrO_2 and $IrCl_3$ have been studied. The results not only improve on the accuracy of published data, but also expand the binding energy database of other iridium core-levels. The difference between anhydrous and hydrated materials is explored and the effect on curve fitting discussed, together with the derivation of suitable line shapes for peak fitting of data acquired from a conventional monochromatic Al K_α X-ray source.

Introduction

Iridium has found application in a wide range of technological fields. Its heat and corrosion resistance means iridium is introduced as an alloying agent in deep-underwater piping, where a iridium-titanium alloys are used[1]. Equally it is used as an alloying agent to harden platinum and also finds use in medical applications, such as cardiovascular stents[2].

Similarly, iridium oxide (IrO_2) has attracted great interest by virtue of its low resistivity and chemical inertness. [3, 4] IrO_2 has been shown to catalyse the oxidation of both NO and CO[5] and the partial oxidation of methane to syngas[6].

Furthermore, in a world where there is a demand for the lowering of greenhouse gases, cleaner fuel sources are required[7] and iridium oxide and related compounds have found major application in water oxidation catalysis[1, 8, 9], with many studies focusing on IrO_2 and IrO_2-RuO_2 composites for use in electrochemical systems for water splitting[10].

Clearly, the diverse uses of iridium compounds necessitates a detailed understanding of the surface chemistry and accurate determination of the surface species, of which there is still exists a debate in the literature[11-13] resulting in poorly fitted spectra.[14, 15]

In addressing peak-fitting models, Payne *et al*.[13] performed a combined hard x-ray photoelectron spectroscopy (HAXPES) and density-functional theory (DFT) study on pelletized IrO_2 in a study to investigate its electronic structure, and generated XPS line shapes and peak positions consistent with screened and unscreened final states. More recently, the results from an elegant XPS, DFT and Near-Edge X-ray Absorption Fine Structure (NEXAFS) study by Preifer *et al*.[11, 12] presented peaks models for amorphous and rutile-like IrO_2, composed of both screened and unscreened photoemission states together with evidence for Ir(III) defect sites.

In both these studies, line shapes were derived for the core-level lines as a function of probed-depth; however, what is apparent from application of these parameters to data collected from a conventional

monochromatic laboratory source, as shown in this paper, is that they are not entirely and directly translatable to common laboratory sources. Furthermore, as these studies focus on the electronic structure of Ir and IrO_2, they understandably focus on the Ir(4f) core-levels, but as will be shown, valuable information is also contained in the O(1s) spectra.

Table 1 shows the mean binding energy and standard deviation derived from inspection of the National Institute for Science and Technology (NIST) XPS database. From the data it is evident the binding energy values for Ir(4f) states have a small deviation (table 1), although very few entries exist for other core-levels, such as the readily accessible Ir(4d) states. Consequently, in this study we expand on this database by inclusion of other core-levels, which are given within the paper and expanded further in table S1 of the supplementary information.

Experimental

X-ray photoelectron spectra were collected using two spectrometers, allowing assessment of the transferability of derived line shapes.

The first system is a Kratos Axis Ultra spectrometer, equipped with a delay line detector (DLD). Spectra were acquired using a monochromatic Al Kα source operating at 144 W power (12 mA x 12 kV) and at pass energies of 10 and 20 eV for high resolution spectra and 160 eV for survey spectra. Spectra were acquired in the hybrid spectroscopy mode over an area approximately 700 x 300 microns. Where applicable charge compensation was achieved using the Kratos immersion lens system.

The second system is a Thermo Scientific K-Alpha$^+$ spectrometer. Spectra were acquired using a monochromatic Al source operating at 72 W (6 mA x 12 kV) with identical pass energies to the Kratos system for high resolution scans and 150 eV for survey scans. The analysis area was an elliptical area of 400 microns. Where required, charge compensation was achieved using the K-Alpha charge neutralisation system, which employs a combination of both electrons and low energy argon ions for charge neutralisation.

Both systems were calibrated to the Au($4f_{7/2}$) signal at 83.95 eV, with the energy dispersion adjusted to yield a binding energy of 932.63 eV for the metallic Cu($2p_{3/2}$) signal. For both systems, spectra requiring charge neutralisation were subsequently calibrated to the C(1s) line at 284.8 eV.

Anhydrous and hydrated IrO_2 samples were obtained from Alfa Aesar (Premion, 99.99%) and used without further treatment. Iridium foil (99.9% purity) was obtained from Goodfellow and analysed after argon sputtering (4kV, 10μA sample current). Anhydrous $IrCl_3$ and $IrCl_3.nH_2O$ were purchased from Alfa Aesar (Premion 99.99% and 99.8% purity respectively) and used as received. For the Kratos system, all powdered samples were mounted in a dry nitrogen-purged glove bag directly above the fast entry lock of the spectrometer to minimise potential atmospheric contamination, whilst for the Thermo system, samples were prepared in a dry-nitrogen atmosphere and placed inside a K-Alpha Vacuum Transfer Module (VTM) which was evacuated to *ca.* 10^{-2} mbar for transfer to the spectrometer.

Samples were also characterised using scanning electron microscopy (SEM), Raman spectroscopy and x-ray diffraction (XRD); these results are presented in the supplementary information (Figure S1).

Data analysis was performed using CasaXPS (v2.3.17) utilising a Shirley background. Peak fits were achieved using Functional Lorentzian (LF) and Gaussian-Lorentzian (GL) lineshapes; more information on the LF lineshape is presented in the supplementary information. Modified Wagner sensitivity

factors and Scofield sensitivity factors were used for the Kratos and Thermo systems respectively, the energy dependence of the Thermo system was 0.6.

Results and Discussion

Iridium Metal

Figure 1 shows the Ir(4f) and (3d) core levels for sputter cleaned Ir foil and reveals an asymmetric doublet ($4f_{7/2}$ at 60.8 eV) with a splitting of 3.0 eV. Fitting is achieved, as for many platinum group metals, with an asymmetric line shape as described in Table 2, suitable for use in CasaXPS. Note that this is different from that derived by Pfeifer *et al*. in their HAXPES study[12] and is more suitable for a conventional monochromatic lab source. A comparison of the two line shapes is given in the supplementary information, figure S2.

It is common to overlook the presence of the Ir($5p_{1/2}$) peak situated under the main Ir(4f) peak envelope, which is *ca.* 15 eV from the $5p_{3/2}$ peak, with only a few studies explicitly addressing this component.[11-13, 16, 17] Although the contribution of the Ir($5p_{1/2}$) peak to the Ir(4f) spectrum is small (estimated to be less than 5%[12]),it should be included in the curve-fitting; to do this it is recommended to increase the Ir(4f) acquisition range to encompass the Ir($5p_{3/2}$) component also and to fit the 5p peaks with the expected 2:1 ratio, equal FWHM values, and a separation of 15.0 eV (figure 1).

For fitting, a Shirley-type background over a relatively small range (*ca.* 57 – 70 eV) should be used, as extension of the background to the higher binding energy side of the 4f doublet leads to significant over estimation of the peak area, which is confirmed by comparison of the corrected peak ratios for Ir(4f) and Ir(4d) peaks as a function of increasing background range. Analysis of the Ir(4d) level should be primarily focused on the $4d_{5/2}$ peak, as inclusion of the $4d_{3/2}$ peak with a Shirley background may not satisfactorily define the background between the peaks; this is true for all compounds studied herein. Remarkably for the many of the compounds analysed a simple GL(70) lineshape satisfactorily defines the peak and we attribute this to the conducting nature of those samples.

Iridium(IV) Oxide, IrO_2

Anhydrous and dihydrate forms of IrO_2 have been studied since it has been shown previously that for ruthenium dioxide (RuO_2), another rutile oxide, the degree of hydration has a significant influence on the core-level peak envelope and associated satellite structure.[18, 19] Unsurprisingly for IrO_2, parallels have been made with RuO_2 and consequently different oxidation states of Ir have been proposed at the surface.[15]

Figure 2(a) shows the Ir(4f) and O(1s) spectra for both forms of IrO_2 and clearly reveal distinct differences in the broadness of the envelope for both core-levels, reflecting a similar behaviour to that of RuO_2.[18, 20, 21] Fitted spectra are shown in figure 2(b) with fitting parameters given in tables 2 and 3.

To address the differences, we first consider the apparently simpler spectra observed for anhydrous IrO_2. XRD and Raman analysis of the oxide reveals a rutile like lattice (supplementary information, Figure S1) which is free of metallic or other crystalline contaminant features.

It has been shown that single crystal IrO_2 exhibits asymmetry in both Ir(4f) and O(1s) core levels, arising as a result of the same conduction electrons screening both Ir(4f) and O(1s) core-holes therefore, we

can potentially model both core-levels with screened and unscreened photoemission states as show in figure 2(b). Note that the line shapes employed here are different to those of Pfiefer *et al*.[11, 12] which are suitable for HAXPES studies, but are clearly not translatable to a standard monochromatic source, as shown in supplementary material, figure S2.

For the hydrated oxide, XRD analysis revealed an amorphous structure, whilst the XPS spectra exhibit a much broader envelope for both iridium and oxygen core-levels (figure 2(a)). It is noted that XRD also shows sharp reflections for metallic Ir, but these are not observed in the Ir(4f) spectra, indicating the dispersion is low, or there is a sufficiently thick oxide shell on the metallic particles so that the metal signal is not observed.

For amorphous IrO_2 samples, recent HAXPES studies have indicated the presence of Ir(III) states, which lie at a binding energy *ca.* 0.5 eV *higher* than the main photoemission peak, which also has screened satellite states.[11, 12] However, the concentration of these states is relatively small and their peaks are not easily separated from data acquired using a conventional monochromatic source. Furthermore, the peak models employed, as observed for the anhydrous sample, are not directly transferrable to data acquired using a conventional monochromatic source.

Despite the presence of minority Ir(III) states, we can be confident that the sample is primarily IrO_2 and the broader envelope Is not due to a discrete phase such as Ir_2O_3 or $Ir(OH)_3$; the former being thermodynamically unfavourable whilst the latter is reported to have a more symmetrical peak profile with a binding energy identical to that of IrO_2 and therefore may be differentiated by spectral inspection alone.[22] The broadening is thus considered to be symptomatic of the small concentration of Ir(III) states together with a different level of atomic separation in the amorphous material when compared to the crystalline counterpart, which results in a difference in the potential experienced by the Ir(4f) core electrons; such observations have been made for molybdenum oxides.[23]

For simplicity of analysis, we present a line shape for the Ir(4f) peak where the core level is modelled by broad asymmetric peaks which encompasses all Ir(IV), Ir(III) and associated satellite states and is shown in figure 2(b); parameters are given in table 2.

Turning attention to the O(1s) levels, it is clear anhydrous IrO_2 also has an asymmetric profile, as highlighted by Wertheim *et al*.,[24] which, as discussed earlier, arises due to the same conductions electrons are responsible for screening the O(1s) and Ir(4f) core-levels. Such asymmetry in the O(1s) core level has not been fully appreciated in many studies, leading to fitting the oxygen peak envelope with multiple Gaussian-like curves such as those observed by Hall and Sherwood in their analysis of Ir/IrO_2 electrode systems,[25] wherein they identified 3 oxygen species deduced from fitting Gaussian peaks. Surprisingly, the peaks identified in their study as higher binding energy oxygen species could not be removed by sputtering and therefore clearly highlights the potential errors which can be made through not appreciating the inherent asymmetry of the oxide.

For the anhydrous material the whole O(1s) envelope is due to the lattice oxygen and screened states, and as such we can employ the same asymmetric line shape as for the Ir(4f) region. Using this line-shape model, together with the satellite structure (table 2), it is clear the O(1s) envelope can be shown to consist solely of oxide and satellite; this is supported by an Ir/O ratio of 0.49, in excellent agreement with that based on the expected stoichiometry. This line shape can be readily applied to data collected on both our instruments, strengthening the model as the photoemission spectra should not significantly change between instruments.

For the hydrated oxide, we can again apply this methodology but instead substitute the line shape derived for the corresponding Ir(4f) core-level. Additionally, a peak attributable to hydroxide,

measured here to be at 531.6 eV, is required (table 3). In respect of data already published, it is noted that similar studies of iridium oxides have not appreciated the asymmetric nature of the oxide peak, leading to inclusion of a peak corresponding to low levels of water.[26] Whilst we do not exclusively discount the presence of water in such hydrated materials, we note that the peak assigned to water by, for example, Cruz *et al.* is very broad[26] and is modelled in our peak-fits by the asymmetric tails of the lattice oxygen signal; furthermore the expected Ir/O stoichiometry is retained and suggests the hydrated oxide has a chemisorbed hydroxide layer as opposed to an oxohydroxide or $Ir(OH)_3$ layer[26].

In summary, the reader is reminded this model does not discount the presence of Ir(III) states noted by Pfeifer *et al*.,[11, 12] but instead is an easy to use model for fitting commonly encountered hydrated forms of IrO_2 such as those reported by Cruz *et al*.[26]

Iridium (III) Chloride: anhydrous ($IrCl_3$) and hydrated ($IrCl_3.nH_2O$)

Iridium chloride is a typical precursor to the formation of IrO_2, Ir-based organometallic and alkene complexes[27] . The only known XPS study analyses a comprehensive range of iridium halides, assigning $Ir(4f_{7/2})$ binding energies of 63.1 and 62.5 eV to $IrCl_4$ and $IrCl_3$ respectively; the corresponding Cl(2p) binding energy was reported as 199.4 eV in both systems.[28] However, the study did not publish fitted Cl(2p) spectra and the authors gave no comment on derived stoichiometry or sample purity. Indeed, one of the current authors has previously shown that both anhydrous and hydrated $RuCl_3$ are far from homogeneous compounds,[18] and therefore it is prudent to reanalyse these compounds.

Figure 3 shows the Ir(4f), Cl(2p) and O(1s) regions for both chlorides. For the hydrated form, the Ir(4f) binding energy is in excellent agreement with that of El-Issa *et al*.[28] at 62.4 eV with a spin orbit splitting of 3.0 eV; the $Ir(5p_{3/2})$ peak is observed at 50.2 eV. A smaller doublet is also noted at 71.4 eV (74.4 eV), only visible in the hydrate; although these could be ascribed to Pt or Ni signals[29], the spin-orbit splitting does not match these species. However, the splitting is of similar magnitude (*ca*. 3.0 eV) to that of the main Ir doublet and as such is ascribed to satellite structure, as observed for other transition metal halide core-levels.[30] The Ir(4d) region, like its (4f) counterpart is comprised of two distinct signals, which can be fitted using the lineshapes for IrO_2 and $IrCl_3$ given in table 2.

The chlorine region displays two clear states, with $Cl(2p_{3/2})$ peaks at binding energies of 198.2 and 199.3 eV and a 1.6 eV splitting for both doublets. The latter we attribute to Ir-Cl bonds, an assignment strengthened by an Ir/Cl ratio of 0.34, whilst the lower binding energy peak we assign to hydrated HCl.[18, 31] The oxygen region exhibits a single peak at 533.5 eV, consistent with water in hydrated materials.[32]

For the anhydrous chloride, differences are noted which, in part, mirror those observed for $RuCl_3$[18]. The main $Cl(2p_{3/2})$ peak is again observed at 199.3 eV, whilst the lower binding energy state is strongly diminished and downshifted slightly to 197.8 eV. The $Ir(4f_{7/2})$ binding energy of for the Ir-Cl bond is found by fitting to be equal to the hydrated sample (62.4 eV) and the Ir/Cl ratio of the peaks is again found to be 0.34. However asymmetric structure at higher binding energy is clearly noted and fitted to 62.7 eV using the line-shape employed for the equivalent oxides, which was chosen based on signals observed in the O(1s) region as discussed below.

The O(1s) region exhibits 3 distinct components at 530.4, 531.8 and 533.4 eV which we assign as oxide, hydroxide and water respectively[26, 33]. The Ir_{Oxide}/O_{530eV} ratio is found to be 0.49 supporting an assignment of an oxide phase which was based on the extra asymmetry in the Ir(4f) region. With the addition of the $Ir_{chloride}/Cl_{199eV}$ ratio (0.34), it is clear there are 2 discrete phases and we propose the

anhydrous chloride has a capping oxide layer which itself is hydroxylated, but does not form for example, a discrete $Ir(OH)_3$ phase, neither do we believe the formation of an oxohydroxide as proposed by Cruz *et al.*[26] and is consistent with a direct hydrolysis route of the chloride,[34] highlighting the hygroscopic nature of the anhydrous chloride. Fitting parameters for iridium, chlorine and oxygen regions are given in table 3.

Conclusions

We have presented an updated analysis of technologically important iridium compounds and highlighted the differences between the photoelectron spectra based on the hydration of the materials and proposed suitable line shapes for their analysis.

It has been demonstrated that:

1. Already published lineshapes are not applicable to common laboratory monochromatic X-ray sources and suitable lineshapes have been derived for two major core levels.
2. The transferability of the derived lineshapes and subsequent quantification between systems from different manufactures has been shown and highlights there is no strong dependence on instrumental factors.
3. For iridium oxides, the asymmetric nature of the oxide component of the O(1s) level as often been overlooked leading to erroneous assignments of species in the literature.
4. Iridium chlorides, depending on their level of hydration reveal different surface chlorine species and anhydrous forms of the chloride have an iridium oxide layer.

Additionally, the available database of binding energies has been increased by inclusion of other iridium core levels.

It is hoped the models presented will allow for improved spectral interpretation of iridium core-level spectra.

Acknowledgments

The authors wish to acknowledge support from Cardiff University as part of the MaxNet consortium. Dr Albert Carley is thanked for his helpful discussions and assistance in the preparation of this manuscript.

Tables

Table 1. Mean binding energies (in eV) as compiled from NIST [29] for Ir, IrO_2 and $IrCl_x$.

Material	**Ir ($4f_{7/2}$) / eV**		**Ir ($4d_{5/2}$) / eV**		**Ir Oxidation State**
	Mean	Standard Deviation	Mean	Standard Deviation	
Ir	60.8	0.2	296.3	N/A	0
$IrCl_x$	62.2	0.7	297.8	0.6	+3
IrO_2	61.9	0.7	N/A	N/A	+4

Table 2. Derived XPS line shapes, binding energies and fitting parameters for Ir, IrO_2 and $IrCl_3$, recorded at 20 eV pass energy, suitable for use with CasaXPS.

Sample	Peak	Binding Energy / eV	Area / %	Doublet Separation / eV	FWHM / eV ¥	CasaXPS Fitting Parameter & Comments
Ir	$4f_{7/2}$	60.8	57.2	3.0	0.84	LF(0.6,1,150,300)
	$4f_{5/2}$	63.8	42.8		0.86	
	$5p_{3/2}$	48.1	66.7	15.0	2.84	GL(30)
	$5p_{1/2}$	63.1	33.3		2.84	
	$4d_{5/2}$	296.2	60.1	15.9	4.20	GL(70) - Fit $4d_{5/2}$ only
	$4d_{3/2}$	312.1	39.9		4.29	
IrO_2 (Anhydrous)	$4f_{7/2}$	61.9	49.5	3.0	0.70	LF(0.3,1,65,100) GL(90) for satellites
	$4f_{5/2}$	64.9	37.1		0.75	
	$4f_{7/2}$ (satellite)	63.2	7.7	3.0	3.64	
	$4f_{5/2}$ (satellite)	66.2	5.8		3.64	
	$5p_{3/2}$	49.7	66.8	15.0	3.90	GL(30)
	$5p_{1/2}$	64.7	33.2		3.90	
	$4d_{5/2}$	298.1	60.2	15.8	4.96	GL(70) - Fit $4d_{5/2}$ only
	$4d_{3/2}$	313.9	39.8		5.24	
IrO_2 (Hydrated)	$4f_{7/2}$	62.5	57.2	3.0	1.60	LF(0.3,1.5,25,150)
	$4f_{5/2}$	65.5	42.8		1.65	
	$5p_{3/2}$	50.2	66.8	15.0	3.88	GL(30)
	$5p_{1/2}$	65.2	33.2		3.88	
	$4d_{5/2}$	298.6	60.1	15.8	4.64	GL(70) - Fit $4d_{5/2}$ only
	$4d_{3/2}$	314.4	39.9		5.00	
$IrCl_3$ (Hydrated)	$4f_{7/2}$	62.6	56.1	3.0	0.94	LF(1,1,55,200)
	$4f_{5/2}$	65.6	42.0		1.05	
	$4f_{7/2}$ (satellite)	71.6	1.1	3.0	1.24	GL(30)
	$4f_{5/2}$ (satellite)	74.6	0.8		1.24	
	$5p_{3/2}$	49.7	66.8	15.0	2.96	GL(30)
	$5p_{1/2}$	64.7	33.2		2.96	
	$4d_{5/2}$	298.1	60.1	15.8	3.92	LF(1.2,0.7,25,280)
	$4d_{3/2}$	313.9	39.9		4.28	
$IrCl_3$ (Anhydrous)*	$4f_{7/2}$	62.4	57.2	3.0	0.94	LF(1,1,55,200)
	$4f_{5/2}$	65.4	42.8		1.05	
	$5p_{3/2}$	49.9	66.8	15.0	3.30	LF(1.2,0.7,25,280)
	$5p_{1/2}$	64.9	33.2		3.30	
	$4d_{5/2}$	297.8	60.1	15.8	3.92	LF(1.2,0.7,25,280)
	$4d_{3/2}$	313.6	39.9		4.28	

* Only Ir-Cl values for the chloride are shown, Ir-O bonds (see text) are those for hydrated IrO_2..

¥ FWHM are presented +/- 0.2 eV; under the conditions used the Kratos spectrometer has a slightly better resolution at equivalent pass energies

FWHM = Full Width at Half Maximum.

Table 3. O(1s) and Cl(2p) fitting parameters for iridium oxides and chlorides; spectra acquired using 20 eV pass energy

Material	Peak	BE / eV	FWHM / eV ¥	CasaXPS Fitting Parameter
IrO2 (Anhydrous)	O(1s) – Oxide	530.0	0.64	LF(0.3,1,65,100)
	O(1s) – Satellite	531.3	2.16	GL(90)
IrO2 (Hydrated)	O(1s) – Oxide	530.5	1.71	LF(0.3,1.5, 25,150)
	O(1s) - Hydroxide	531.6	1.50	GL(30)
	O(1s) - Water	532.9	1.60	GL(30)
IrCl3 (Hydrated)	O(1s) - Water	533.6	2.21	GL(30)
	Cl(2p) - Chloride	199.0	1.08	GL(30)
	Cl(2p) – HCl	198.0	1.05	GL(30)
IrCl3 (Anhydrous)	O(1s) – Oxide	530.3	1.42	LF(0.3,1.5,25,150)
	O(1s) – Hydroxide	532.0	1.70	GL(30)
	O(1s) - Water	533.6	1.70	GL(30)
	$Cl(2p_{3/2})$ - Chloride	199.2	1.25	GL(30)
	$Cl(2p_{3/2})$ – HCl	197.7	1.25	GL(30)

¥ FWHM are presented +/- 0.2 eV; under the conditions used the Kratos spectrometer has a slightly better resolution at equivalent pass energies

FWHM = Full Width at Half Maximum

Figures

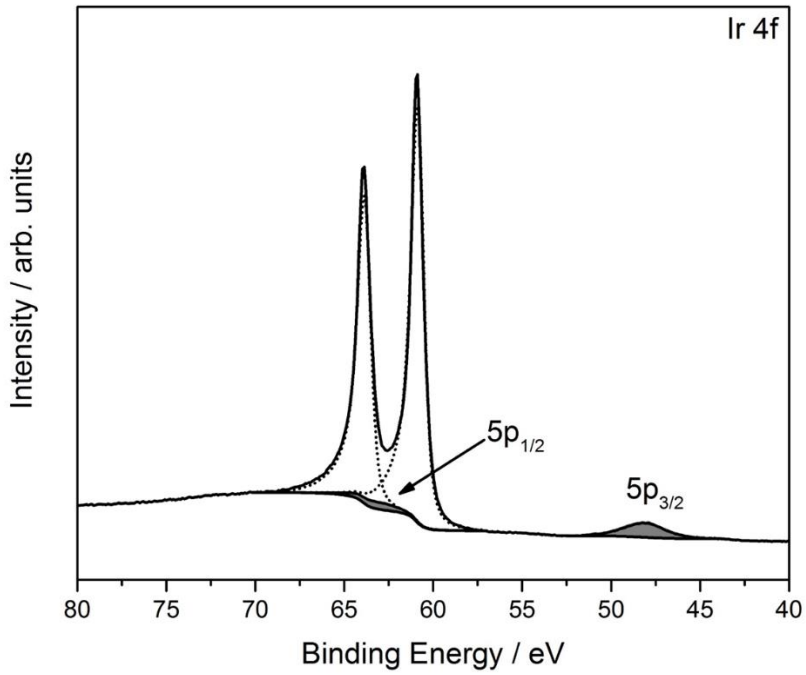

Figure 1. Fitted Ir(4f)/Ir(5p) core-level spectra for sputter cleaned iridium foil.

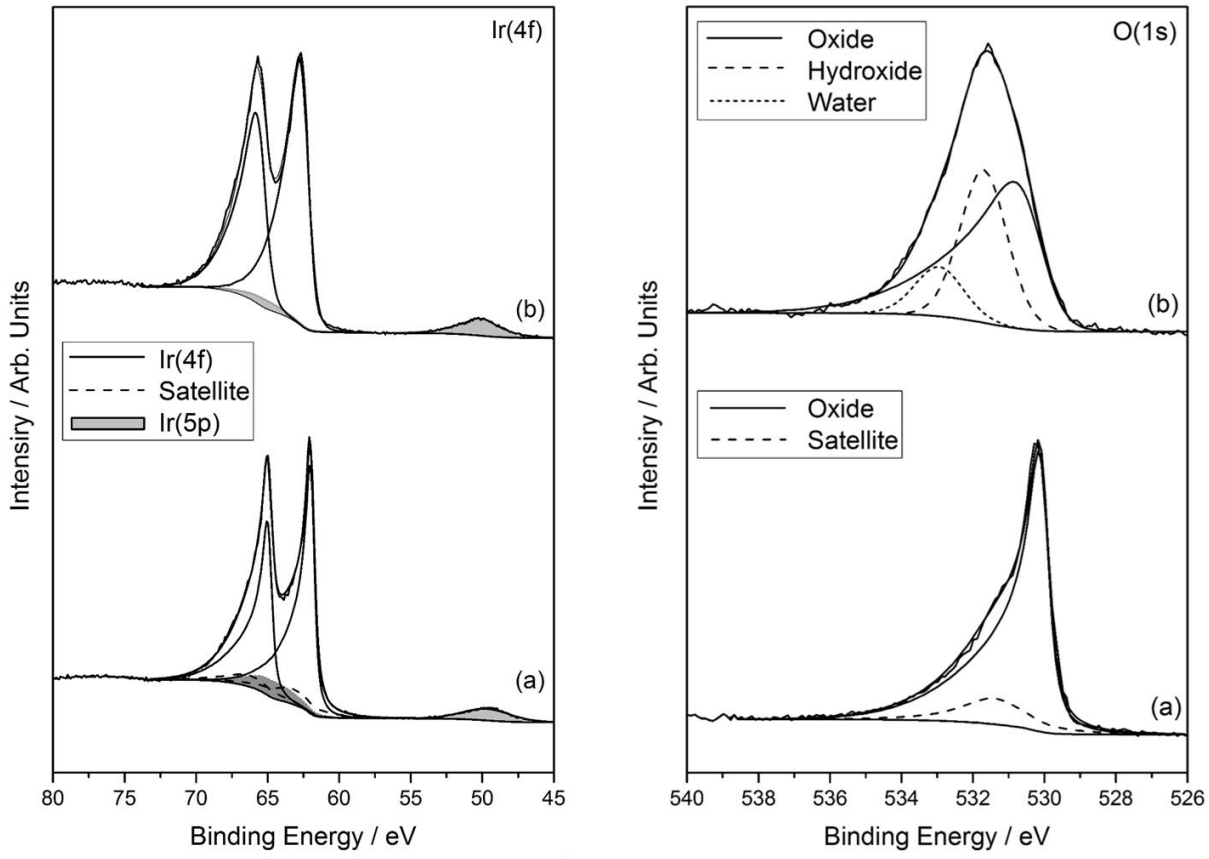

Figure 2. Ir(4f) and O(1s) core-level spectra for (a) anhydrous IrO_2 and (b) $IrO_2.2H_2O$

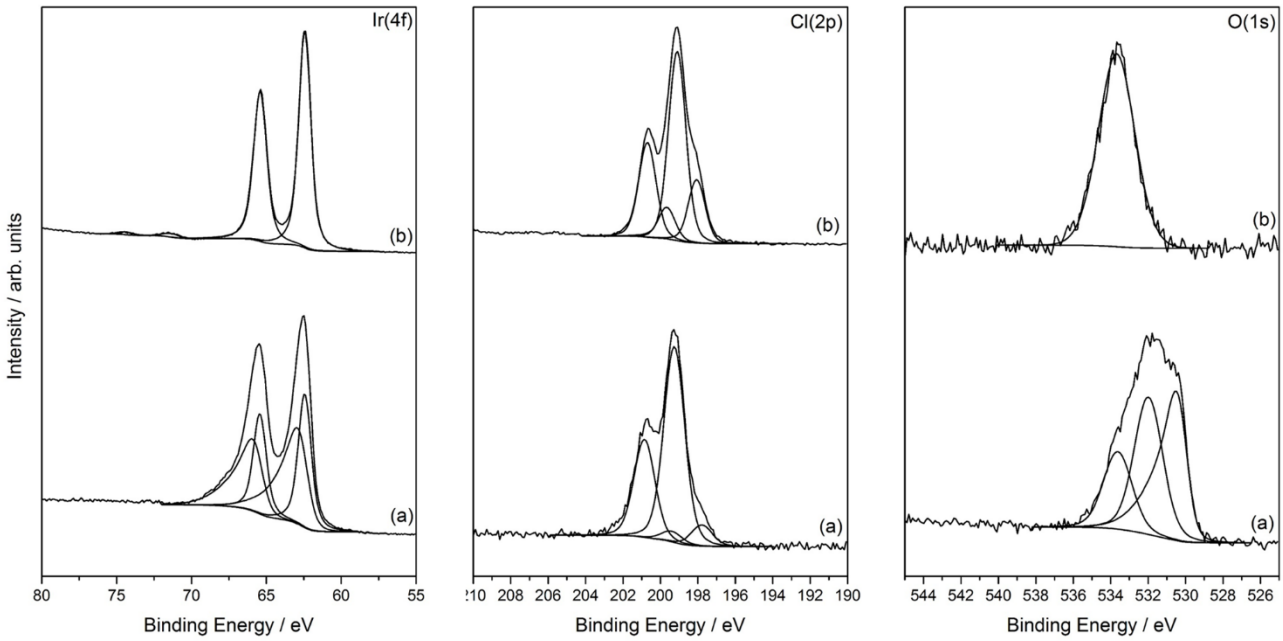

Figure 3. Ir(4f), Cl(2p) and O(1s) spectra for (a) $IrCl_3$ and (b) $IrCl_3.nH_2O$. For clarity of the Ir(4f) spectra, Ir(5p) signals are not shown.

References

[1] M. Li, Y. B. Wang, X. Zhang, Q. H. Li, Q. Liu, Y. Cheng, Y. F. Zheng, T. F. Xi, S. C. Wei, *Mater Sci Eng C Mater Biol Appl* **2013**, *33*, 15.

[2] L. Atanasoska, P. Gupta, C. Deng, R. Warner, S. Larson, J. Thompson, *ECS Trans* **2009**, *16*, 37.

[3] C. U. Pinnow, I. Kasko, N. Nagel, T. Mikolajick, C. Dehm, F. Jahnel, M. Seibt, U. Geyer, K. Samwer, *J Appl Phys* **2002**, *91*, 1707.

[4] T. Nakamura, Y. Nakao, A. Kamisawa, H. Takasu, *Jpn J Appl Phys* **1994**, *33*, 5207.

[5] J. F. Weaver, *Chem Rev* **2013**, *113*, 4164.

[6] K. Nakagawa, N. Ikenaga, T. Suzuki, T. Kobayashi, M. Haruta, *Appl Catal, A* **1998**, *169*, 281.

[7] S. Dunn, *Int J Hydrogen Energy* **2002**, *27*, 235.

[8] S. W. Sheehan, J. M. Thomsen, U. Hintermair, R. H. Crabtree, G. W. Brudvig, C. A. Schmuttenmaer, *Nat Commun* **2015**, *6*, 6469.

[9] R. D. L. Smith, B. Sporinova, R. D. Fagan, S. Trudel, C. P. Berlinguette, *Chem Mater* **2014**, *26*, 1654.

[10] T. Audichon, T. W. Napporn, C. Canaff, C. Morais, C. Comminges, K. B. Kokoh, *J Phys Chem C* **2016**, *120*, 2562.

[11] V. Pfeifer, T. E. Jones, J. J. V. Velez, C. Massue, M. T. Greiner, R. Arrigo, D. Teschner, F. Girgsdies, M. Scherzer, J. Allan, M. Hashagen, G. Weinberg, S. Piccinin, M. Havecker, A. Knop-Gericke, R. Schlogl, *PCCP* **2016**, *18*, 2292.

[12] V. Pfeifer, T. E. Jones, J. J. Velasco Vélez, C. Massué, R. Arrigo, D. Teschner, F. Girgsdies, M. Scherzer, M. T. Greiner, J. Allan, M. Hashagen, G. Weinberg, S. Piccinin, M. Hävecker, A. Knop-Gericke, R. Schlögl, *Surf Interface Anal* **2016**, *48*, 261.

[13] J. M. Kahk, C. G. Poll, F. E. Oropeza, J. M. Ablett, D. Ceolin, J. P. Rueff, S. Agrestini, Y. Utsumi, K. D. Tsuei, Y. F. Liao, F. Borgatti, G. Panaccione, A. Regoutz, R. G. Egdell, B. J. Morgan, D. O. Scanlon, D. J. Payne, *Phys Rev Lett* **2014**, *112*, 117601.

[14] R. S. Chen, Y. S. Huang, Y. M. Liang, D. S. Tsai, Y. Chi, J. J. Kai, *J Mater Chem* **2003**, *13*, 2525.

[15] G. Q. Wei, Y. X. Wang, C. D. Huang, Q. J. Gao, Z. T. Wang, L. Xu, *Int J Hydrogen Energy* **2010**, *35*, 3951.

[16] Y. X. Liu, H. Masumoto, T. Goto, *Mater Trans* **2004**, *45*, 900.

[17] R. Nyholm, A. Berndtsson, N. Martensson, *J Phys C: Solid State Phys* **1980**, *13*, L1091.

[18] D. J. Morgan, *Surf Interface Anal* **2015**, *47*, 1072.

[19] A. Foelske, O. Barbieri, M. Hahn, R. Kötz, *Electrochem Solid-State Lett* **2006**, *9*, A268.

[20] I. M. Kodintsev, S. Trasatti, M. Rubel, A. Wieckowski, N. Kaufher, *Langmuir* **1992**, *8*, 283.

[21] M. Hara, K. Asami, K. Hashimoto, T. Masumoto, *Electrochim Acta* **1983**, *28*, 1073.

[22] S. Kato, J. U. Jung, T. Suenobu, S. Fukuzumi, *Energy Environ Sci* **2013**, *6*, 3756.

[23] J. Baltrusaitis, B. Mendoza-Sanchez, V. Fernandez, R. Veenstra, N. Dukstiene, A. Roberts, N. Fairley, *Appl Surf Sci* **2015**, *326*, 151.

[24] G. K. Wertheim, H. J. Guggenheim, *Phys Rev B* **1980**, *22*, 4680.

[25] H. Y. Hall, P. M. A. Sherwood, *J Chem Soc Farad T 1* **1984**, *80*, 135.

[26] A. M. Cruz, L. Abad, N. M. Carretero, J. Moral-Vico, J. Fraxedas, P. Lozano, G. Subias, V. Padial, M. Carballo, J. E. Collazos-Castro, N. Casan-Pastor, *J Phys Chem C* **2012**, *116*, 5156.

[27] F. A. Cotton, G. Wilkinson, *Advanced Inorganic Chemistry*, 5th Edition ed., John Wiley & Sons, Chichester, England, **1988**.

[28] B. D. El-Issa, A. Katrib, R. Ghodsian, B. A. Salsa, S. H. Addassi, *Int J Quantum Chem* **1988**, *33*, 195.

[29] A. V. Naumkin, A. Kraut-Vass, S. W. Garrenstroom, C. J. Powell, National Institute of Standards and Technology, Gaithersburg, **2012**.

[30] B. W. Veal, A. P. Paulikas, *Phys Rev B Condens Matter* **1985**, *31*, 5399.

[31] A. G. Wren, R. W. Phillips, L. U. Tolentino, *J Colloid Interface Sci* **1979**, *70*, 544.

[32] Y. I. Kim, W. E. Hatfield, *Inorg Chim Acta* **1991**, *188*, 15.

[33] R. P. Vasquez, *J Electron Spectrosc Relat Phenom* **1991**, *56*, 217.

[34] J. Kristóf, J. Mihály, S. Daolio, A. De Battisti, L. Nanni, C. Piccirillo, *J Electroanal Chem* **1997**, *434*, 99.